

**Supplementary Information for "Biases in active land water storage capacity and water limitation of evapotranspiration in CMIP6 models"**  
 Francesco Giardina<sup>1</sup>, Ryan S. Padrón<sup>1,2</sup>, Benjamin D. Stocker<sup>3,4</sup>, Dominik L. Schumacher<sup>1</sup>,  
 Sonia I. Seneviratne<sup>1</sup>

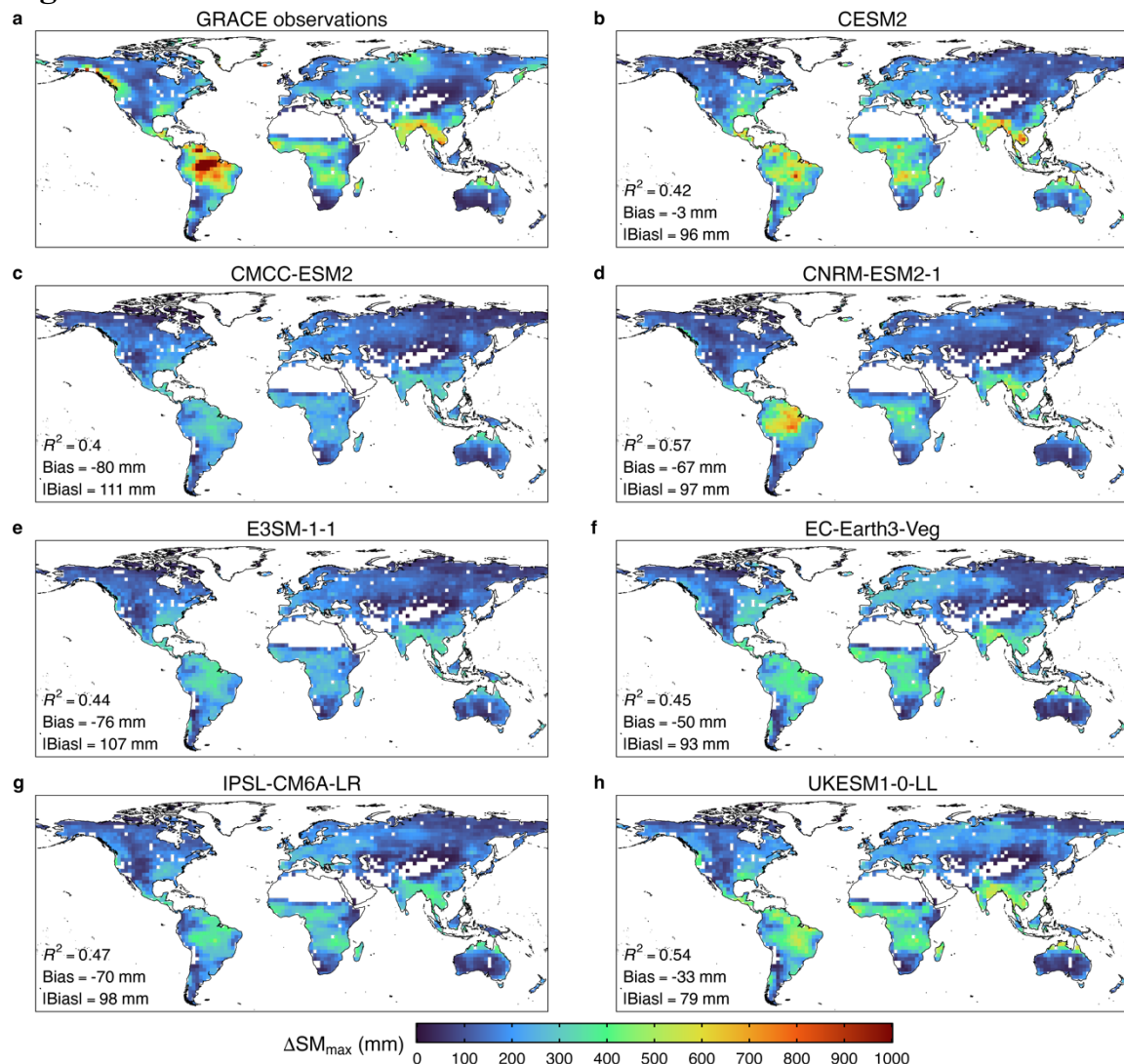
**Tables**

**Table S1 | CMIP6 model information**

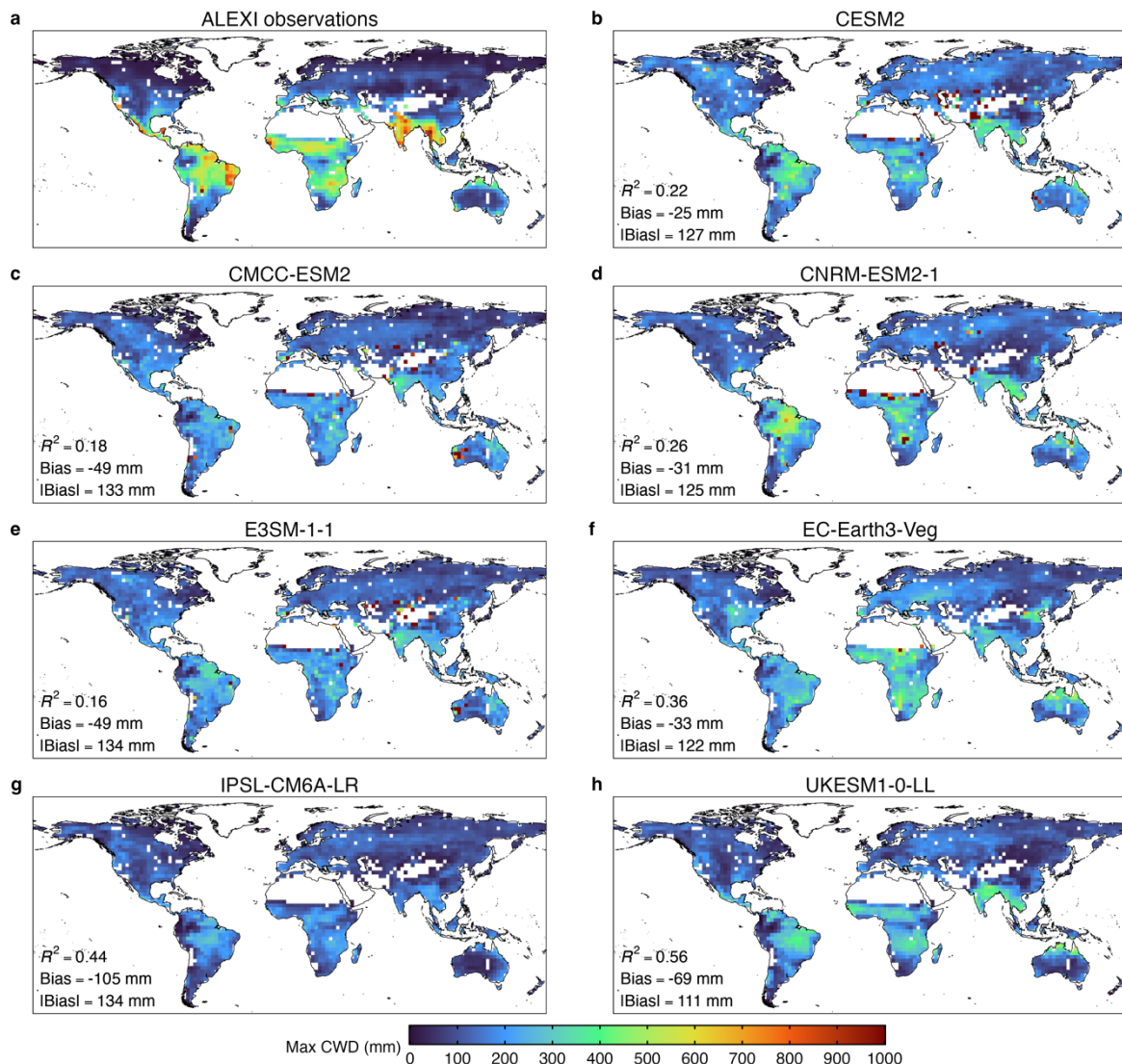
ESM Acronym	Run ID	References	Notes
CESM2	r1i1p1f1	Kennedy et al. [2019] <sup>1</sup> Lawrence et al. [2019] <sup>2</sup>	<ul style="list-style-type: none"> <li>representation of LAI dynamics (LAI seasonality is not constant)</li> <li>representation of water stress based on leaf water potential</li> </ul>
CMCC-ESM2	r1i1p1f1	Cherchi et al. [2019] <sup>3</sup>	<ul style="list-style-type: none"> <li>no representation of vegetation properties</li> <li>interactive terrestrial carbon-cycle processes</li> </ul>
CNRM-ESM2-1	r1i1p1f2	Séférian et al. [2019] <sup>4</sup>	<ul style="list-style-type: none"> <li>representation of LAI dynamics (LAI seasonality is not constant)</li> <li>interactive vegetation properties</li> <li>interactive terrestrial carbon-cycle processes</li> </ul>
E3SM-1-1	r1i1p1f1	Leung et al. [2020] <sup>5</sup>	-
EC-Earth3-Veg	r1i1p1f1	Döscher et al. [2022] <sup>6</sup>	<ul style="list-style-type: none"> <li>interactive vegetation properties</li> <li>interactive terrestrial carbon-cycle processes</li> </ul>
IPSL-CM6A-LR	r1i1p1f1	Boucher et al. [2020] <sup>7</sup>	<ul style="list-style-type: none"> <li>representation of LAI dynamics (LAI seasonality is not constant)</li> <li>interactive vegetation properties</li> <li>interactive terrestrial carbon-cycle processes</li> </ul>
UKESM1-0-LL	r1i1p1f2	Sellar et al. [2020] <sup>8</sup>	<ul style="list-style-type: none"> <li>representation of LAI dynamics (LAI seasonality is not constant)</li> <li>land use change in dynamic vegetation simulations</li> <li>interactive vegetation cover</li> </ul>

Table partially adapted from Ref<sup>9</sup>

## Figures

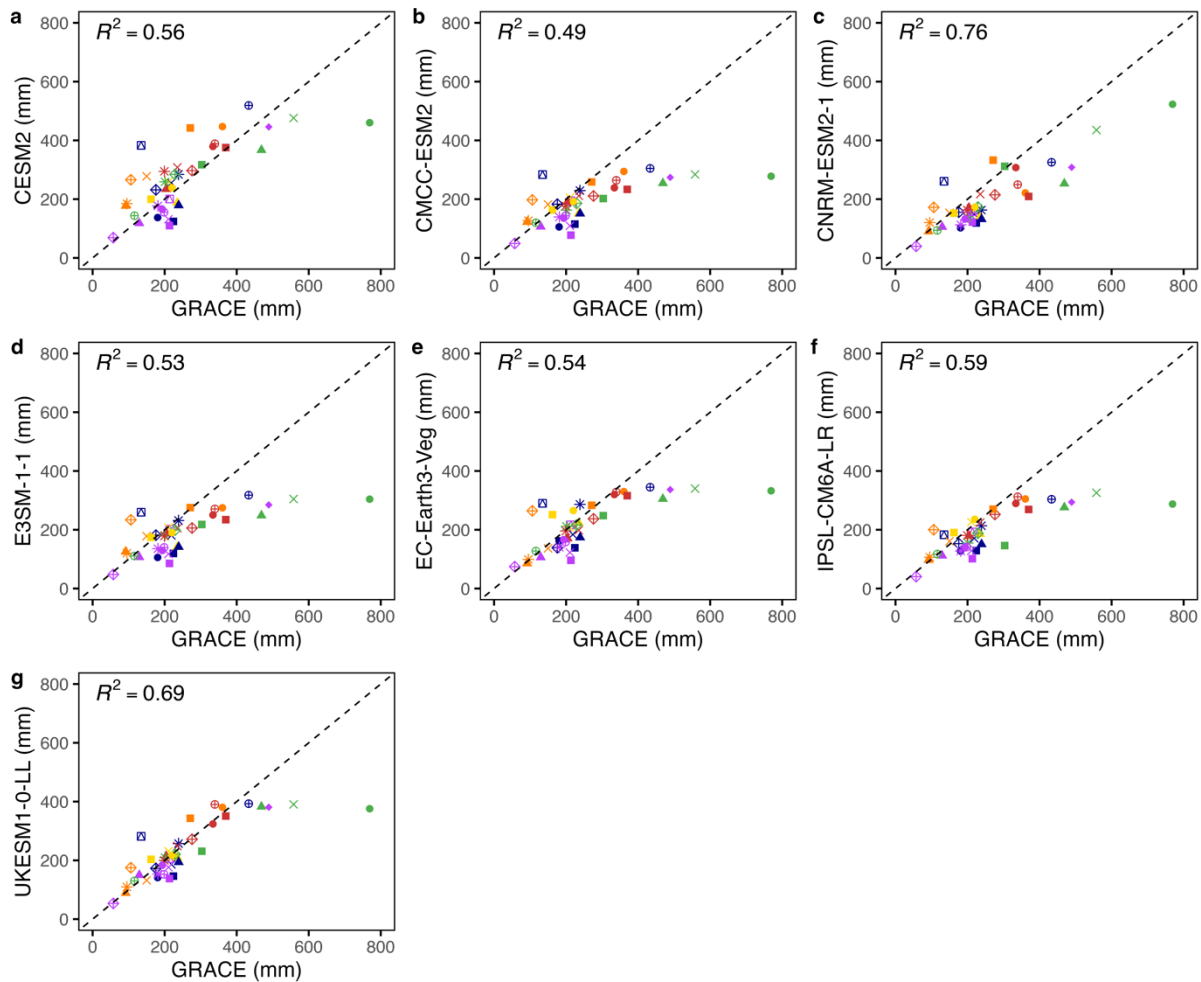


**Fig. S1 | Comparison of long-term maximum annual soil moisture depletion ( $\Delta SM_{max}$ ) between GRACE observations and LMIP-CMIP6 simulations.**  $\Delta SM_{max}$  was first derived for every year during 2003-2014. The maximum yearly reduction across those years was retained. **a**,  $\Delta TWS_{max}$  from GRACE. **b-h**,  $\Delta SM_{max}$  from LMIP-CMIP6. The *land-hist* simulation was used across CMIP6 models. Bilinear interpolation was applied to harmonize the GRACE resolution with that of CMIP6. The raw bias was determined by subtracting pixel-by-pixel the observed value from each model and then calculating the mean of these differences across all pixels. For the absolute bias, we computed the mean after taking the absolute value of each pixel-wise subtraction. Biases were weighted to account for the latitudinal variation in grid cell area. Values exceeding 1000 mm are colored as 1000 mm for clarity. Values exceeding 1000 mm colored as 1000 mm for clarity.



**Fig. S2 | Comparison of maximum cumulative water deficit ( $CWD_{max}$ ) derived from ALEXI and WATCH-WFDEI observations versus LMIP-CMIP6 simulations.** **a**, Maximum CWD determined from ALEXI and WATCH-WFDEI observations, augmented using an extreme value distribution with an 80-year return period, as detailed in Ref<sup>10</sup>. **b-h**, Maximum CWD assessed over the 80 years of LMIP-CMIP6 data (1935-2014), to align with the methodology used for the observational data. Biases were weighted to account for the latitudinal variation in grid cell area. Values exceeding 1000 mm are colored as 1000 mm for clarity. Values exceeding 1000 mm are colored as 1000 mm clarity.

$\Delta SM_{max}$ : maximum depletion of total-column soil moisture



IPCC WGI reference regions

- |                     |                     |                   |                   |                   |                     |                     |             |                     |                   |                     |                          |                     |                     |                   |            |                       |            |                 |                  |                  |                    |                    |                     |                     |              |                  |             |             |                    |            |            |                   |          |               |               |               |               |               |
|---------------------|---------------------|-------------------|-------------------|-------------------|---------------------|---------------------|-------------|---------------------|-------------------|---------------------|--------------------------|---------------------|---------------------|-------------------|------------|-----------------------|------------|-----------------|------------------|------------------|--------------------|--------------------|---------------------|---------------------|--------------|------------------|-------------|-------------|--------------------|------------|------------|-------------------|----------|---------------|---------------|---------------|---------------|---------------|
| ■ N.W.North-America | ● N.E.North-America | ▲ W.North-America | × C.North-America | * E.North-America | ◊ N.Central-America | ⊕ S.Central-America | □ Caribbean | ■ N.W.South-America | ● N.South-America | ▲ N.E.South-America | × South-American-Monsoon | * S.W.South-America | ◊ S.E.South-America | ⊕ S.South-America | □ N.Europe | ○ West&Central-Europe | ■ E.Europe | ○ Mediterranean | ■ Western-Africa | ● Central-Africa | ▲ N.Eastern-Africa | × S.Eastern-Africa | * W.Southern-Africa | ◊ E.Southern-Africa | ⊕ Madagascar | ■ Russian-Arctic | ● W.Siberia | ▲ E.Siberia | × Russian-Far-East | * W.C.Asia | ◊ E.C.Asia | ○ Tibetan-Plateau | ■ E.Asia | ● N.Australia | ▲ C.Australia | × E.Australia | * S.Australia | ◊ New-Zealand |
|---------------------|---------------------|-------------------|-------------------|-------------------|---------------------|---------------------|-------------|---------------------|-------------------|---------------------|--------------------------|---------------------|---------------------|-------------------|------------|-----------------------|------------|-----------------|------------------|------------------|--------------------|--------------------|---------------------|---------------------|--------------|------------------|-------------|-------------|--------------------|------------|------------|-------------------|----------|---------------|---------------|---------------|---------------|---------------|

**Fig. S3 | Comparative analysis of long-term maximum annual soil moisture depletion across different IPCC regions based on LMIP-CMIP6 model simulations and observations.** We present a region-wise evaluation of long-term maximum annual soil moisture depletion, using GRACE data and corresponding LMIP-CMIP6 model simulations. We first determined the long-term maximum annual soil moisture depletion in every pixel and then we calculated the mean of this value within each IPCC region for model and observational data.

### Maximum Cumulative Water Deficit over a 80-year period

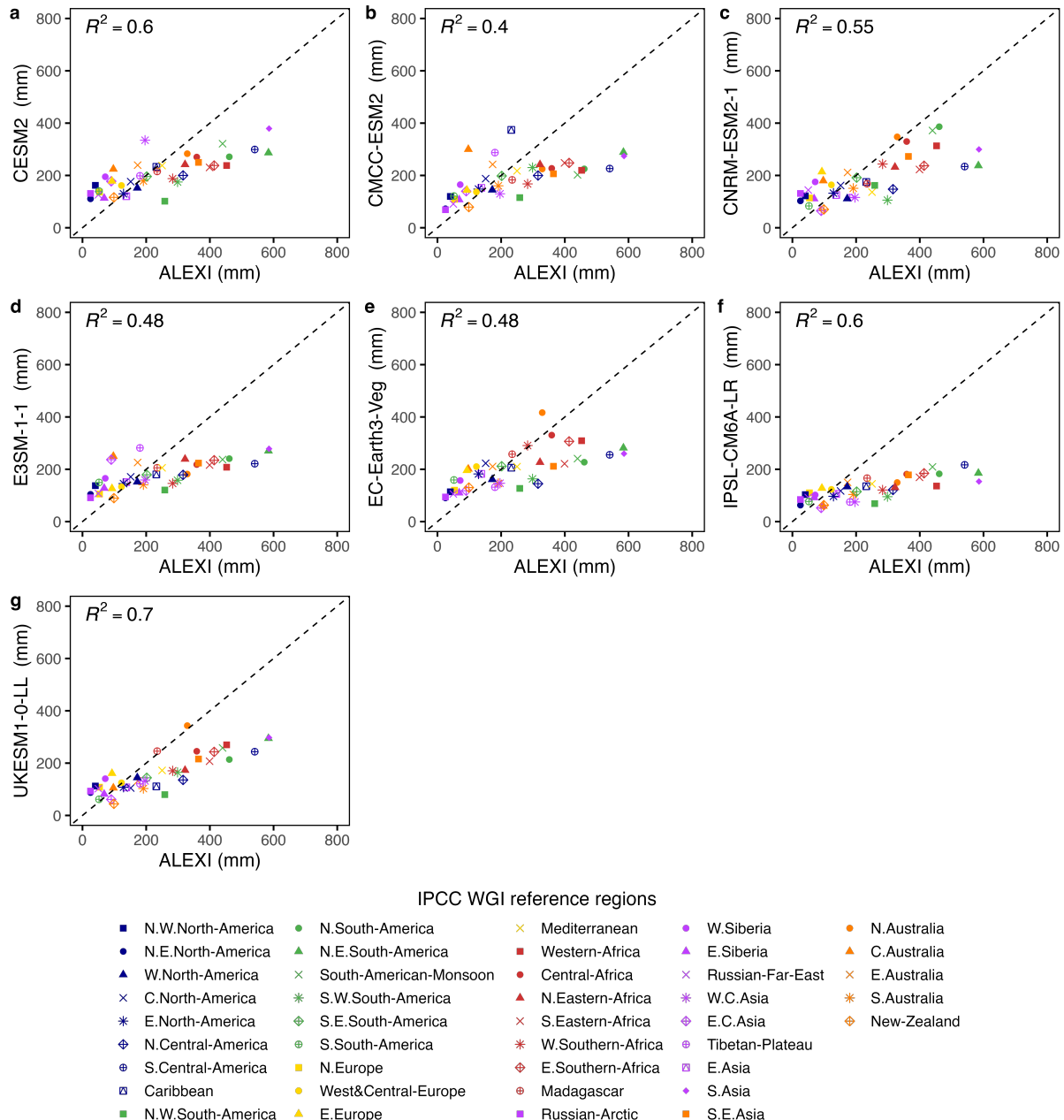


**Fig. S4 | Comparative analysis of maximum cumulative water deficit ( $CWD_{max}$ ) across different IPCC regions based on LMIP-CMIP6 model simulations and observations.** We present a region-wise evaluation of  $CWD_{max}$ , using ALEXI and WATCH-WFDEI data, and corresponding LMIP-CMIP6 model simulations. We first determined  $CWD_{max}$  in every pixel and then we calculated the mean of this value within each IPCC region for model and observational data.

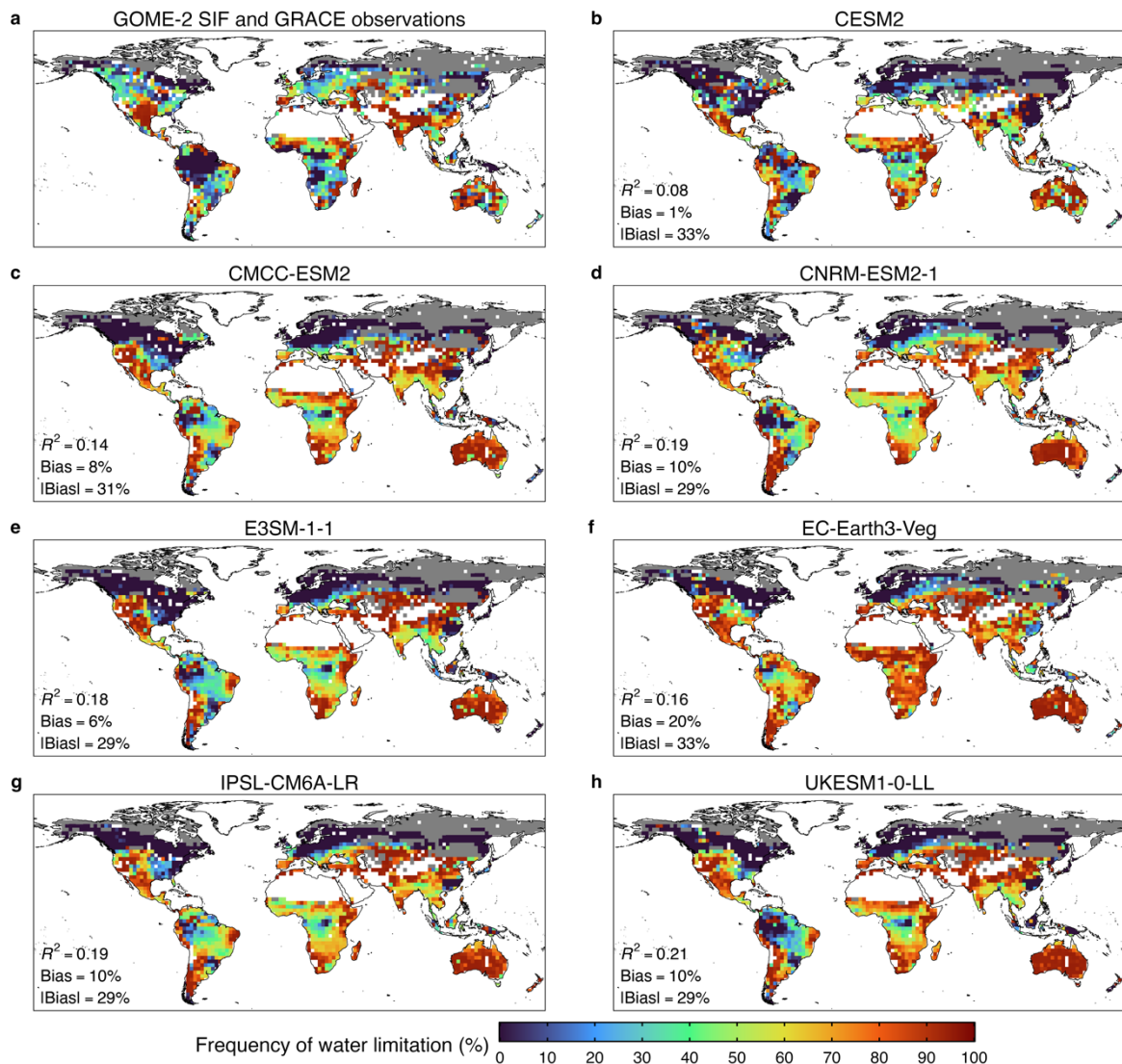


**Fig. S5 | Global maps of frequency of water limitation.** Pixel-specific critical water limitation thresholds ( $\theta_{\text{crit}}$ ) were first calculated to determine when plant water stress occurs. We then show the fraction of months with total-column soil moisture below  $\theta_{\text{crit}}$ . **a**,  $\theta_{\text{crit}}$  determined with the normalized observational solar-induced fluorescence (SIF; a proxy for photosynthesis) versus normalized terrestrial water storage (TWS; the sum of soil moisture and groundwater, surface water, snow and ice) from the Gravity Recovery and Climate Experiment (GRACE, 2007-2014). **b-h**,  $\theta_{\text{crit}}$  calculated with the evaporative fraction (EF) vs normalized total-column soil moisture with LMIP-CMIP6 data (2007-2014). Dark blue pixels represent areas where water is rarely limiting. On the other hand, dark red pixels represent areas that are almost always water-limited. Grey areas illustrate regions where the segmented regression could not be applied due to scarcity of data points. The raw bias was determined by subtracting pixel-by-pixel the observed value from each model and then calculating the mean of these differences across all pixels. For the absolute bias, we computed the mean after taking the absolute value of each pixel-wise subtraction. Biases were weighted to account for the latitudinal variation in grid cell area. Details of all datasets and normalizations can be found in the Methods.

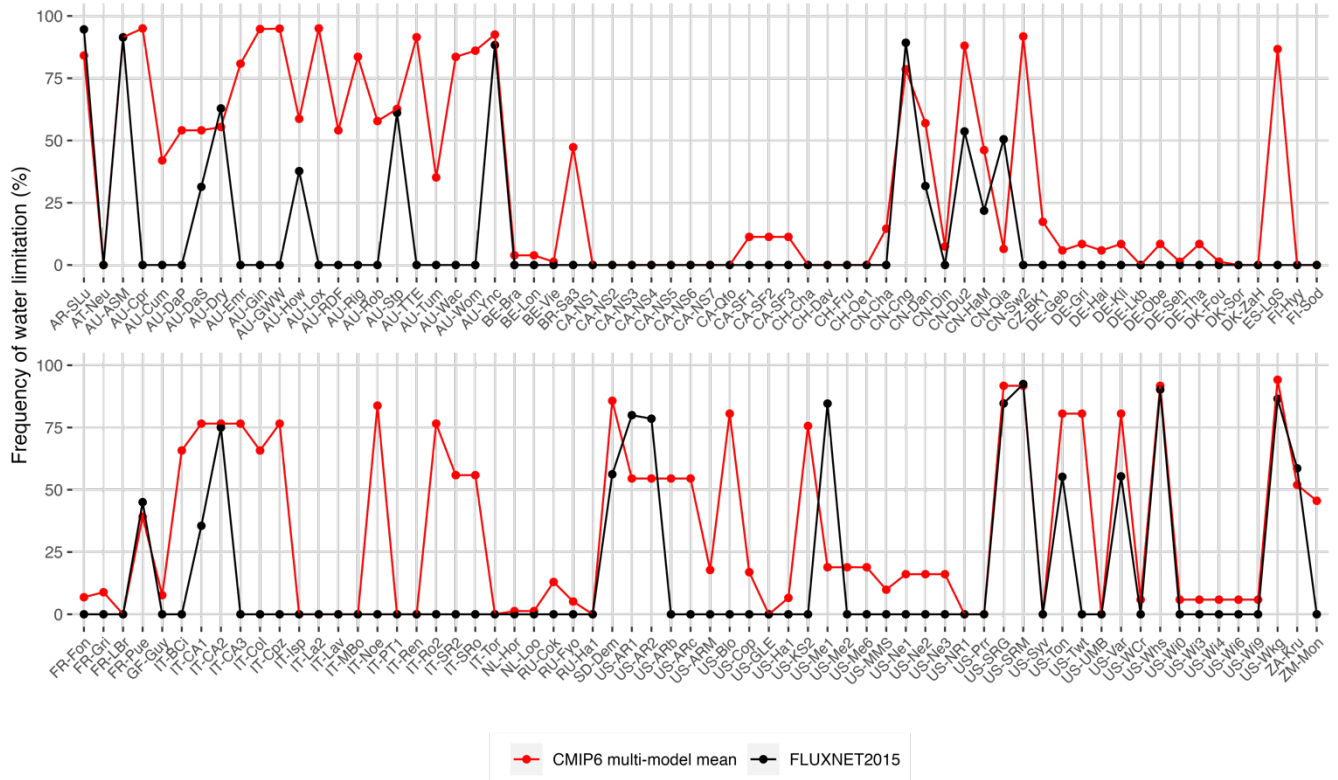


**Fig. S6 | Frequency of water limitation at FLUXNET2015 sites.** The red dotted line corresponds to the LMIP-CMIP6 multi-model mean, whereas the black dotted line to the FLUXNET2015 data. The multi-model mean was calculated from models UKESM1-0-LL, IPSL-CM6A-LR, EC-Earth3-Veg, and CNRM-ESM2-1, which were the only models in our selection providing daily data of the relevant variables (see Methods).

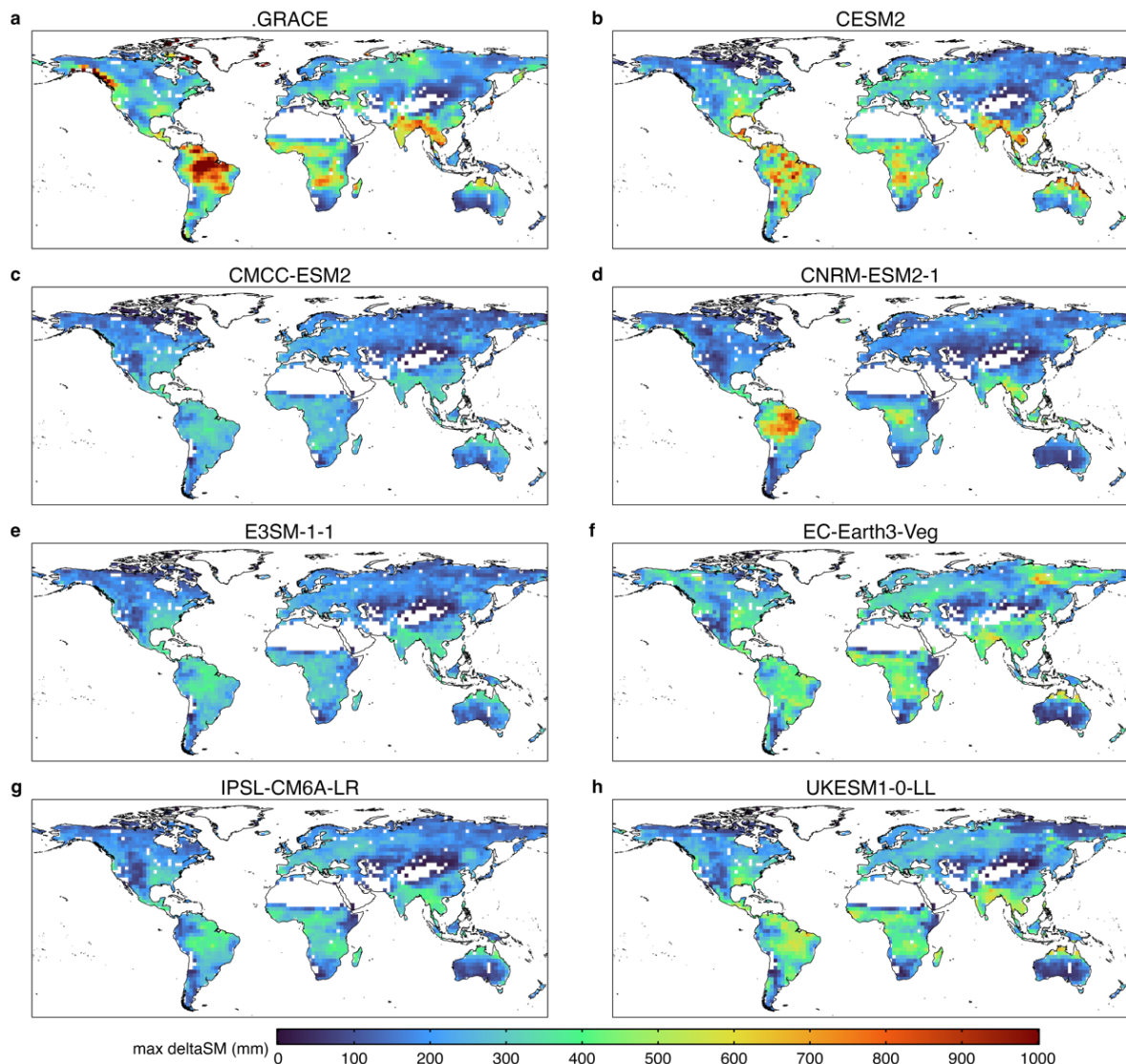


**Fig. S7 | Comparison of long-term maximum multi-year soil moisture depletion ( $\Delta SM_{max}$ ) between GRACE observations and LMIP-CMIP6 simulations.**  $\Delta SM_{max}$  was directly calculated over the entire time period 2003–2014. **a**,  $\Delta TWS_{max}$  from GRACE. **b-h**,  $\Delta SM_{max}$  from LMIP-CMIP6. The *land-hist* simulation was used across CMIP6 models. Bilinear interpolation was applied to harmonize the GRACE resolution with that of CMIP6. The mean bias was calculated by first computing the bias between model data and GRACE at every pixel, and then calculating the mean of all biases for the entire globe. Values exceeding 1000 mm colored as 1000 mm to address outliers.

## References

1. Kennedy, D. *et al.* Implementing Plant Hydraulics in the Community Land Model, Version 5. *J Adv Model Earth Syst* **11**, 485–513 (2019).
2. Lawrence, D. M. *et al.* The Community Land Model Version 5: Description of New Features, Benchmarking, and Impact of Forcing Uncertainty. *J Adv Model Earth Syst* **11**, 4245–4287 (2019).
3. Cherchi, A. *et al.* Global Mean Climate and Main Patterns of Variability in the CMCC-CM2 Coupled Model. *J Adv Model Earth Syst* **11**, 185–209 (2019).
4. Séférian, R. *et al.* Evaluation of CNRM Earth System Model, CNRM-ESM2-1: Role of Earth System Processes in Present-Day and Future Climate. *J Adv Model Earth Syst* **11**, 4182–4227 (2019).
5. Leung, L. R., Bader, D. C., Taylor, M. A. & McCoy, R. B. An Introduction to the E3SM Special Collection: Goals, Science Drivers, Development, and Analysis. *J Adv Model Earth Syst* **12**, e2019MS001821 (2020).
6. Döscher, R. *et al.* The EC-Earth3 Earth system model for the Coupled Model Intercomparison Project 6. *Geosci Model Dev* **15**, 2973–3020 (2022).
7. Boucher, O. *et al.* Presentation and Evaluation of the IPSL-CM6A-LR Climate Model. *J Adv Model Earth Syst* **12**, e2019MS002010 (2020).
8. Sellar, A. A. *et al.* Implementation of U.K. Earth System Models for CMIP6. *J Adv Model Earth Syst* **12**, e2019MS001946 (2020).
9. Brands, S. A circulation-based performance atlas of the CMIP5 and 6 models for regional climate studies in the Northern Hemisphere mid-to-high latitudes. *Geosci Model Dev* **15**, 1375–1411 (2022).
10. Stocker, B. D. *et al.* Global patterns of water storage in the rooting zones of vegetation. *Nat Geosci* **16**, 250–256 (2023).